Journal of Engineering Sciences, Assiut University, Vol. 40, No 2, pp. 533-555, March 2012

SENSORLESS TORQUE CONTROL OF AN IPMSM DRIVE TAKING IRON LOSS AND SATURATION INTO ACCOUNT

A. M. El-Sawy, and E. G. Shehata
Electrical Eng. Dept., Faculty of Engineering, El -Minia University, Egypt
E-mail: sawy1980@yahoo.com

(Received January 4, 2012 Accepted January 19, 2012)

This paper presents a novel direct torque control (DTC) of a sensorless interior permanent magnet synchronous motor (IPMSM). The speed and position of the IPMSM are estimated online based on active flux concept. The active flux estimation needs the quadrature axis self inductance value. The conventional two axes machine model is modified in order to include the influence of the saturation and cross saturation effect on the variation of self and cross coupling inductances in the direct and the quadrature axes. The self and cross coupling inductances values are stored in lookup table in the motor model. In addition, the iron loss is taken into the motor modeling. To overcome the large ripple content associated with the DTC, a torque/flux sliding mode controller (SMC) has been employed. The command voltage is estimated from the torque and flux errors based on the two switching functions. The space vector modulation (SVM) is combined with the SMC to ensure minimum torque and flux ripples and to provide high resolution voltage control. To overcome the stator resistance variation, a fuzzy logic estimator is designed to detect the resistance variation online. The proposed scheme has the advantages of simple implementation, and does not require an external signal injection. In addition, it combines the merits of the DTC, SMC, and SVM beside the sensorless control. Simulation works are carried out to demonstrate the ability of the proposed scheme at different operating conditions. The theoretical results are compared to published results to confirm the high performance of the proposed scheme at standstill, low and high speeds including load disturbance and parameters variation.

***KEYWORDS**: Active flux concept – Speed sensorless control – Direct torque control – Sliding mode control – Space vector modulation.*

1. INTRODUCTION

Controlled electric motor drives without speed sensor have emerged as a mature technology in the past decade [1]. The advantages of sensorless control are reduced hardware complexity, lower cost, reduced size of the drive machine, elimination of the sensor cable, better noise immunity, increased reliability, and less maintenance requirements. A motor without speed sensor is preferred for operation in hostile environments. The advancement in the field of the digital signal processing encourages the speed estimation or detection approach. Many of the speed estimators depend on the motor mathematical model, where, the back emf or the permanent magnet flux is estimated. These methods can be used with the surface mounted PMSM [2]. However,

the anisotropy of the IPMSM increases the model complexity. Where, the stator inductance is a function in the rotor position.

Different algorithms were studied for sensorless control of the IPMSM [3-21]. The popular algorithm utilizes the extended emf estimation in a rotating reference frame [3-5]. This type gives a good performance at medium and high speed operation. However, this type fails at low speed and at standstill operation because the back emf is proportional to the motor speed. A start-up algorithm is required, when the motor is at a standstill or at a low speed. In addition, the measured voltage and current has to be transformed into a new rotating frame.

Another algorithm utilizes the stator inductance variation based on the relative position of the rotor [6-8]. This algorithm gives a good performance at low speed and at standstill operation. However, the generation of the high frequency signal increases the drive complicity and the motor losses. In addition, a negative torque can be generated and degrades the scheme performance. In [6], a high frequency voltage signal/pulse is injected in the stator winding. The position of the rotor is extracted from the measured current signal response. In [7], the inductance matrix including the rotor position information is determined from the current harmonics produced by the switching operations of an inverter driving the IPMSM. Speed information can be obtained from the position information. In [8], the extended emf estimation and the signal injection algorithms are used together for position sensorless control. In this case, the rotor position is estimated by a signal injection algorithm at standstill. After the starting period, the extended emf estimation algorithm is applied.

Speed observers have been employed also in many literatures. Sliding mode observer is used to estimate the motor speed or position based on the estimated flux [9-12]. However, the chattering phenomenon, and the need for high frequency signal injection are the drawbacks of this method. Also, extended Kalman filter [13-15] is employed to estimate the speed of the IPMSM using measured voltage and current signals. However, large computational burden is considered the main disadvantage of this technique. In [16], a linear model of the IPMSM based on the stationary reference frame is constructed. The speed/position observer is designed based on γ- positive real problem. However, large speed error appears at rated value. In addition, the sensorless control at low speed under load torque disturbance can not be realized successfully. In [17], a new observer is constructed based on multi-rate time system which estimates the applied voltage to the motor. In addition, a full order observer is used to estimate the stator flux and therefore the rotor position. However, this algorithm can not be applied at zero speed. In [18], an observer based on the motor model is used to estimate the rotor flux and the motor speed of the induction motor. This method is sensitive to the parameters variation.

In some literatures the induction motor speed was estimated from the stator flux speed and either the load torque angle as in [19] or the slip speed as in [20]. However, the speed error was significant especially at low speed under load disturbance. Also, the motor parameters must be known accurately. Active flux concept [21] was proposed also for speed estimation. This method has the advantages of obtaining wide range of speed control without any signal injection. In addition, it uses a simple algorithm. The variation of L_q due to magnetic saturation was considered.

In this paper, the active flux concept is employed to estimate the motor speed online [21]. The active flux is aligned with the direct axis in the synchronous reference frame. The estimation of the rotor speed based on the active flux needs the quadrature axis self inductance value. The conventional two axes machine model is modified in order to include the influence of the saturation and cross saturation effect on the self and cross coupling inductances in the direct and the quadrature axes. The self and cross coupling inductances values are stored in lookup table in the motor model. The proposed scheme does not require additional complicated algorithms or signal injection schemes especially at very low speed operation. The sensorless estimation algorithm is combined with torque /flux SMC as in Ref. [27] to obtain high performance at wide range of speed operation without motor speed or position measurements. In addition, a fuzzy logic stator resistance estimator is designed to ensure high performance at all speeds. The stator resistance variation is detected based on variation of the stator current vector amplitude. Computer simulations are carried out to evaluate the performance of the proposed scheme. To demonstrate the validity of the proposed scheme, the motor speed, estimated speed and rotor position are compared with those measured previously [11]. The results show that the simulation results of the proposed technique are closer to the measured results of the technique proposed in [11].

2. DYNAMIC IMPSM MODEL TAKING SATURATION AND IRON LOSS INTO ACCOUNT

The equivalent circuit of the IPMSM based on a synchronous d-q reference frame is shown in figure 1. From the equivalent circuit, the dynamic motor model in the synchronous rotating frame taking saturation and iron loss into account was given as [22-24]:

$$V_d = R_s i_d + L_{dd} p i_{dm} + L_{dq} p i_{qm} - \omega_e \lambda_q \tag{1}$$

$$V_q = R_s i_q + L_{qq} p i_{qm} + L_{qd} p i_{dm} + \omega_e \lambda_d \tag{2}$$

where R_s is the stator resistance, V_d, V_q are the voltage components in the synchronous reference frame, i_d, i_q are the line current components in the synchronous reference frame, i_{dm}, i_{qm} are the magnetizing current components and ω_e is the electrical rotor speed.

The stator flux linkage components (λ_d , λ_q) can be written as:

$$\frac{\partial \lambda_d(i_{dm}, i_{qm})}{\partial t} = L_{dd} \frac{\partial i_{dm}}{\partial t} + L_{dq} \frac{\partial i_{qm}}{\partial t} \tag{3}$$

$$\frac{\partial \lambda_q(i_{dm}, i_{qm})}{\partial t} = L_{qq} \frac{\partial i_{qm}}{\partial t} + L_{qd} \frac{\partial i_{dm}}{\partial t} \tag{4}$$

where, L_{dd} and L_{qq} are the direct and quadrature axes self inductances and can be defined as follows:

$$L_{dd} = \frac{\partial \lambda_d(i_{dm}, i_{qm})}{\partial i_{dm}} \approx \left.\frac{\Delta \lambda_d}{\Delta i_{dm}}\right|_{i_{qm}=const} \quad , \quad L_{qq} = \frac{\partial \lambda_q(i_{dm}, i_{qm})}{\partial i_{qm}} \approx \left.\frac{\Delta \lambda_q}{\Delta i_q}\right|_{i_{dm}=const}$$

L_{dq} and L_{dq} are the direct and quadrature axes cross coupling inductances and can be defined as follows:

$$L_{dq} = \frac{\partial \lambda_d(i_{dm}, i_{qm})}{\partial i_{qm}} \approx \left.\frac{\Delta \lambda_d}{\Delta i_{qm}}\right|_{i_{dm}=const} \quad , \quad L_{qd} = \frac{\partial \lambda_q(i_{dm}, i_{qm})}{\partial i_{dm}} \approx \left.\frac{\Delta \lambda_q}{\Delta i_{dm}}\right|_{i_{qm}=const}$$

The magnetizing current components (i_{dm} and i_{qm}) are calculated from the difference between the line current components and the iron loss current components (i_{di} and i_{qi}) and can be expressed as:

$$i_{dm} = i_d - i_{di} \tag{5}$$

$$i_{qm} = i_q - i_{qi} \tag{6}$$

where, in steady state, the d-q iron loss currents components can be written as follows:

$$i_{di} = -\frac{\omega_e \lambda_q}{R_i} \tag{7}$$

$$i_{qi} = \frac{\omega_e \lambda_d}{R_i} \tag{8}$$

where R_i is the core loss resistance. The motor electromagnetic torque can be written in terms of the magnetizing current and flux linkage components as follows:

$$T_e = 1.5P(\lambda_d i_{qm} - \lambda_q i_{dm}) \tag{9}$$

The mechanical equation of IPMSM can be written as follows:

$$p\omega_r = \frac{T_e - T_L - D\omega_r}{J} \tag{10}$$

where D is the damping coefficient.

The stator flux linkage amplitude can be expressed as:

$$\lambda_s = (\lambda_d{}^2 + \lambda_q{}^2)^{0.5} \tag{11}$$

In the equivalent circuit of figure 1, the iron loss per phase is modeled as

$$P_i = R_i(i_{qi}{}^2 + i_{di}{}^2) \tag{12}$$

The value of the core loss resistance can be modeled as a function of the operating frequency and the no-load core loss resistance (R_{io}). The core loss resistance R_i is divided into two parallel resistances for hysteresis losses and eddy current losses, respectively. The hysteresis losses resistance (R_{ih}) is proportional to the frequency and the eddy current resistance (R_{ie}) does not depend on the frequency. Their expressions can be written as follows [23-24]:

$$R_{ih} = R_{iho}\left(\frac{\omega_e}{\omega_b}\right) \tag{13}$$

$$R_{ie} = R_{ieo} \tag{14}$$

$$R_i = R_{ie} + R_{ih} = R_{ieo} + R_{iho}\left(\frac{\omega_e}{\omega_b}\right) \tag{15}$$

The iron loss resistance at different values of motor speeds is drawn in figure 2 [24].

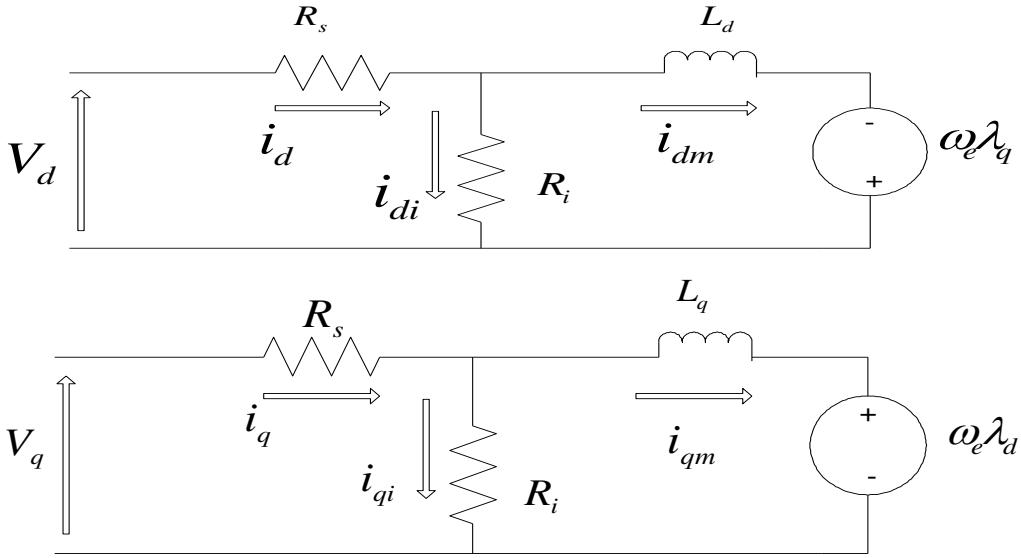

Figure 1: d and q axes equivalent circuits for an IPMSM taking iron loss into account.

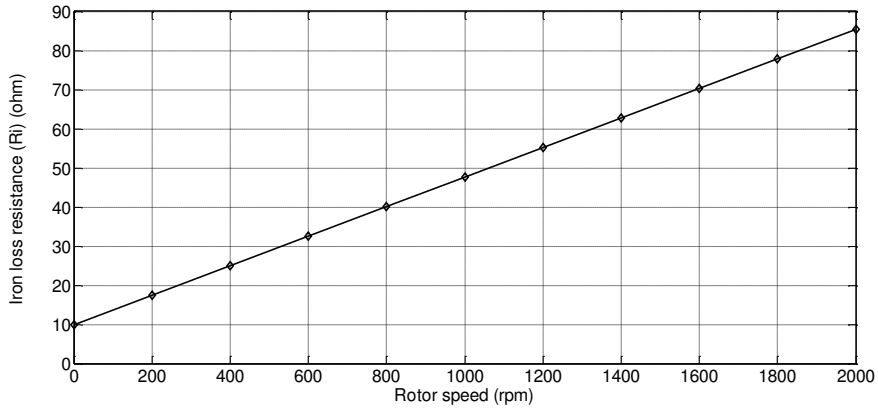

Figure 2: Variation of iron loss resistance with an operating frequency.

Saturation and cross-magnetization modeling of an anisotropic synchronous machine (e.g. IPMSM) requires data regarding direct and quadrature axes magnetizing curves. While the magnetizing curve for the direct axis is generally known, the magnetizing curve for the quadrature axis is usually not available. If both direct and

quadrature axes magnetizing curves are known, then the two saturation factor approach to saturation representation may be utilized [22]. However, in most practical cases quadrature axis magnetizing curve is not available, or it is assumed that direct and quadrature magnetizing curves depend, for a given machine, solely on the resultant magnetizing current. The saturation of machine is in this case usually represented by means of a single saturation factor approach. Consequently, the conventional two-axis machine model is modified in order to include the influence of saturation and cross-coupling effects on the variation of self- and cross-coupling inductances in the direct and in the quadrature axis, which depend on both the direct and the quadrature axis currents. The modified two-axis machine model parameters are evaluated by experiments performed on the IPMSM using a controlled voltage-source inverter [22]. The nonlinear characteristic $\lambda_q(i_{qm}, i_{dm} = const.)$ is presented in figure 3 for one magnetization cycle. For the obtained nonlinear characteristic, the average value of current is calculated for each value of the flux linkage. In this way, the complete curve presented in figure 4 is generated. Figure 5 shows the values of the self and cross coupling inductances for different values of d- and q-axis currents.

3. SPEED ESTIMATION OF THE IPMSM BASED ON ACTIVE FLUX CONCEPT

The concept of active flux for the IPMSM taking iron loss and saturation effect is defined as follows:

$$\lambda_a = \lambda_f + (L_{dd} - L_{qq}) i_{dm} \tag{16}$$

The pervious equation indicates that the active flux vector is aligned with the d-axis of the rotor frame as shown in figure 6.

Using equations (16), one can obtain:

$$\lambda_a = \lambda_d - L_{qq}\, i_{dm} \tag{17}$$

The q- axis stator flux component can be expressed as:

$$0 = \lambda_q - L_{qq}\, i_{qm} \tag{18}$$

Combining equations (17) and (18), the active flux can be described in the space phasor form as:

$$\bar{\lambda}_a = \bar{\lambda}_s - L_q\, \bar{i}_s \tag{19}$$

where $\bar{\lambda}_a$, $\bar{\lambda}_s$, and $\bar{i}_s$ are the active flux , stator flux and stator current space vectors respectively.

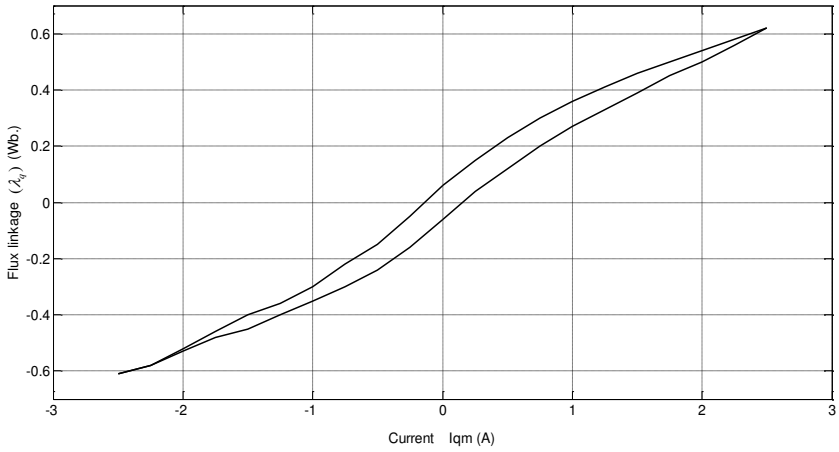

Figure 3: The nonlinear characteristic $\lambda_q(i_{qm}, i_{dm} = const.)$

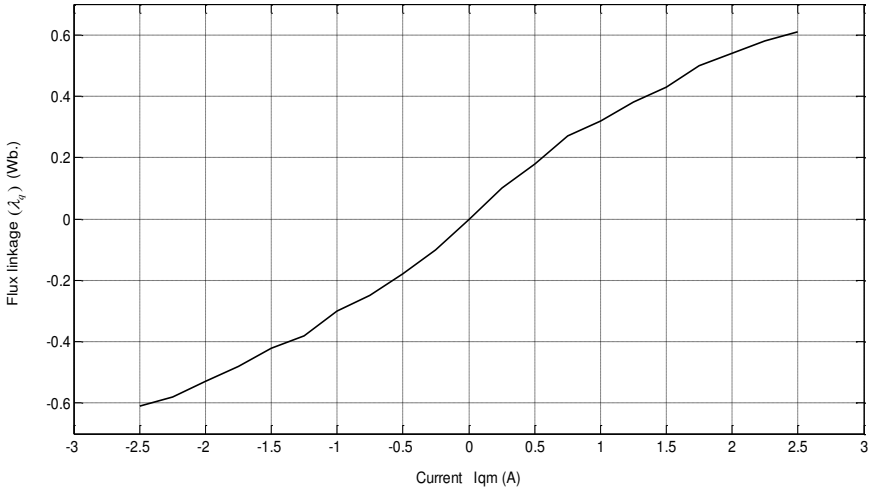

Figure 4: Characteristic $\lambda_q(i_{qm}, i_{dm} = const.)$ i_{qm} is averaged for each λ_q.

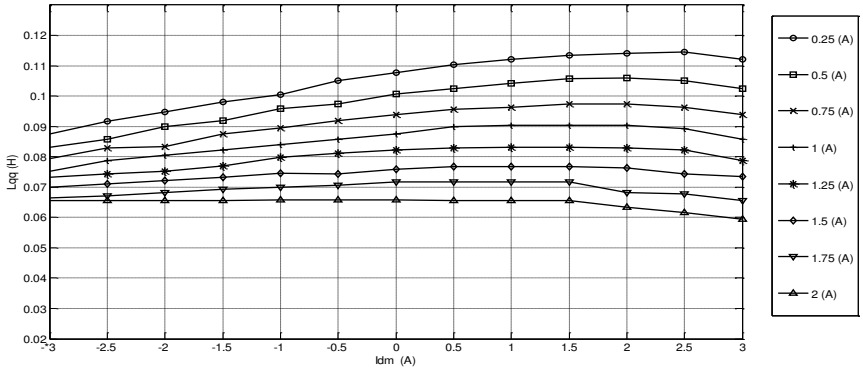

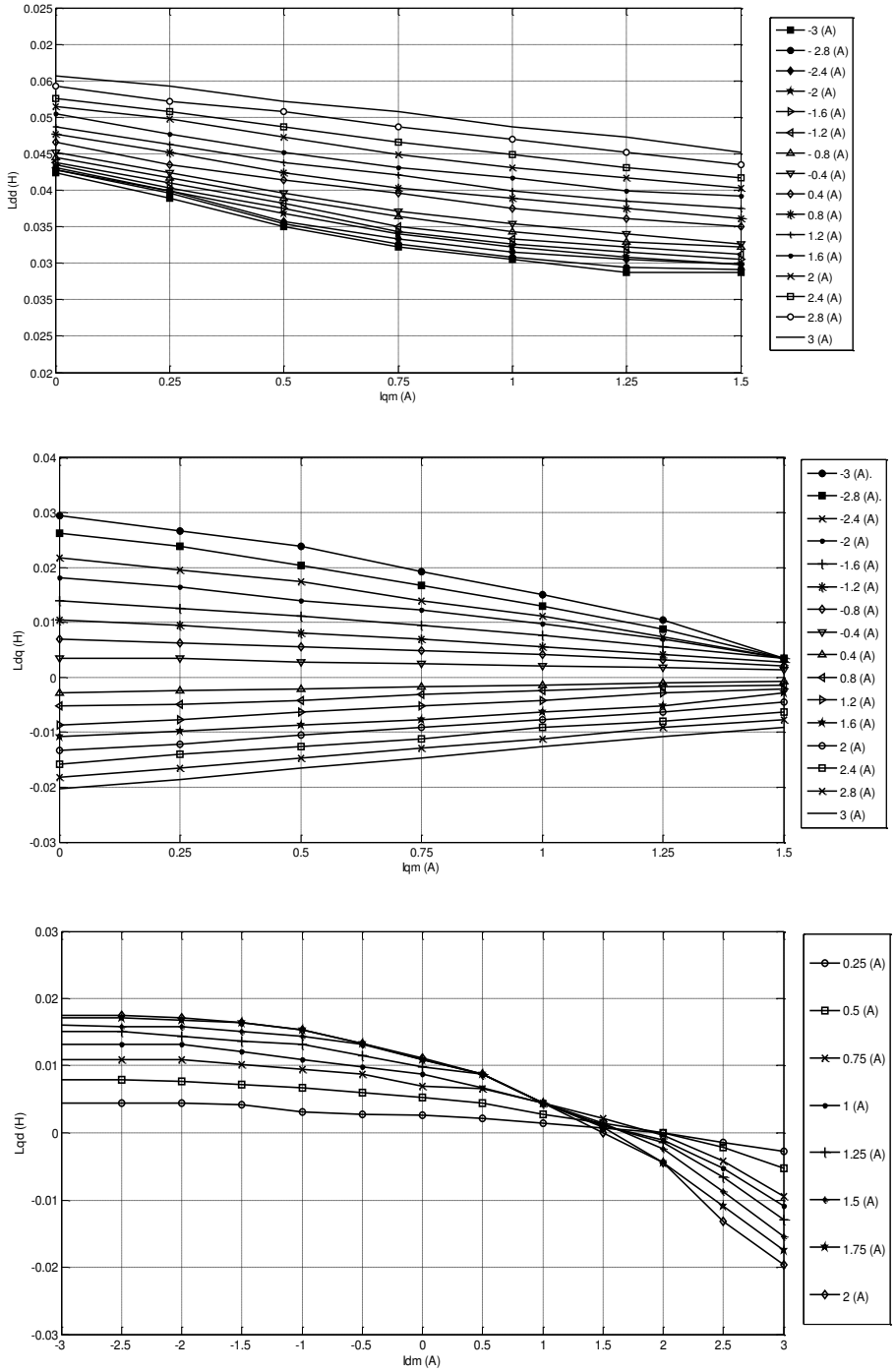

Figure 5: variation of the self and cross coupling inductance with d- and q- currents.

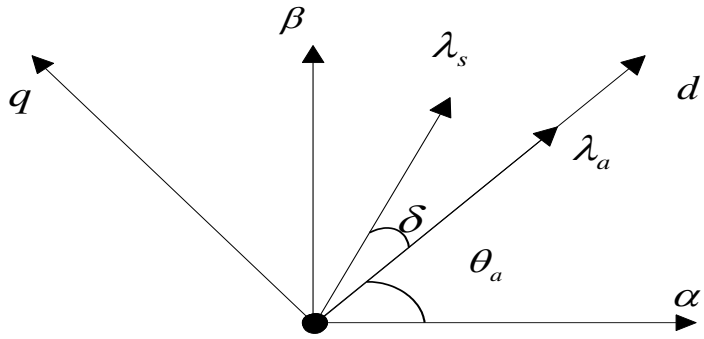

Figure 6: Space position of the stator and active flux vectors.

Substituting the stator flux in equation (19) by the integration of the back emf, the active flux vector becomes:

$$\bar{\lambda}_a = \int (\bar{V}_s - R_s \bar{i}_s)dt - L_{qq}\bar{i}_s \tag{20}$$

Equation (20) indicates that the active flux vector can be estimated using the stator voltage and current space vectors. The active flux can be expressed in the polar form as:

$$\bar{\lambda}_a = \lambda_a \angle \hat{\theta}_a \tag{21}$$

where λ_a , and $\hat{\theta}_a$ are the amplitude and angle of the active flux space vector. The rotor position angle is estimated in terms of active flux components as:

$$\hat{\theta}_a = \tan^{-1}(\frac{\lambda_{\beta a}}{\lambda_{\alpha a}}) \tag{22}$$

where $\lambda_{\alpha a}$ and $\lambda_{\beta a}$ are the stationary components of the active flux in the stator frame.

The motor speed can be estimated in discrete form from the time differentiation of equation (22) as:

$$\hat{\omega}_e = \frac{d\hat{\theta}_a}{dt} = \frac{(\lambda_{\alpha a})_{k-1}.(\lambda_{\beta a})_k - (\lambda_{\beta a})_{k-1}.(\lambda_{\alpha a})_k}{T_s.[(\lambda_{\alpha a})_k^2 + (\lambda_{\beta a})_k^2]} \tag{23}$$

where the active flux components are calculated at the samples k and $k-1$, and T_s is the sampling interval.

The block diagram of the speed estimator is shown in figure 7. In this figure, the rotor position, speed, stator flux linkage and electromagnetic torque are estimated from the measured voltage and current signals. The implementation of the estimator is very simple and does not require any additional computational or external injection.

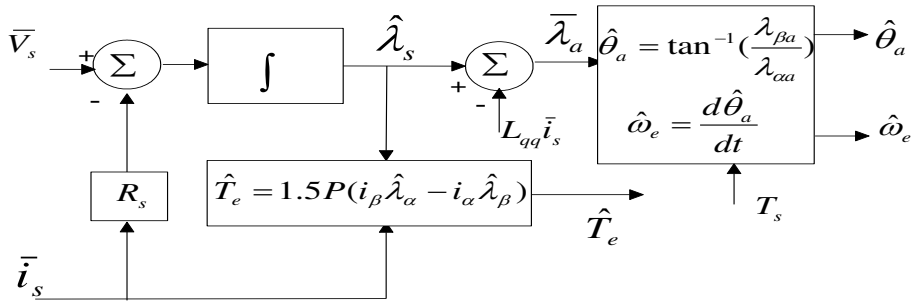

Figure 7: Block diagram of torque, stator flux, rotor speed and position estimator.

4. STATOR RESISTANCE ESTIMATION ALGORITHM BASED ON FUZZY LOGIC ESTIMATOR

The stator resistance changes due to the change in temperature or frequency during the operation of the machine. At high speeds, the stator resistance voltage drop is small compared to the stator voltage. At low speeds, this drop becomes the dominant. Therefore, any change in stator resistance gives wrong estimation of the stator flux and consequently the electromagnetic torque and the stator flux position. An error in stator flux position is more important as it can cause the controller to select a wrong switching state which can result in failure of the controller. Moreover, in the case of sensorless speed control, the mismatched stator resistance introduces an error in the position and speed estimation. Among other variables of the machine, the stator current vector is highly affected by the resistance changes [25-26].

Let the change in the stator resistance be ΔR_s, which causes a Δi_s change in the stator current. The nominal stator resistance is used to estimate stator flux and electromagnetic torque as:

$$\hat{\lambda}_s = \int (V_s - R_s(i_s + \Delta i_s)dt \tag{24}$$

$$\hat{T}_e = 1.5P(\hat{\lambda}_s) \otimes (i_s + \Delta i_s) \tag{25}$$

where " $\otimes$ " denotes the cross product operator.

Considering the change in the stator resistance to be in the machine model, the actual stator flux and electromagnetic torque can be written as follows:

$$\lambda_s = \int (V_s - (R_s + \Delta R_s)(i_s + \Delta i_s)dt \tag{26}$$

$$T_e = 1.5P(\lambda_s) \otimes (i_s + \Delta i_s) \tag{27}$$

The errors in the stator flux and torque due to the change in the stator resistance are given by:

$$\Delta\lambda_s = \lambda_s - \hat{\lambda}_s = -\int \Delta R_s(i_s + \Delta i_s)dt \tag{28}$$

$$\Delta T_e = T_e - \hat{T}_e = 1.5P(\lambda_s - \hat{\lambda}_s) \otimes (i_s + \Delta i_s)$$
$$= 1.5P\left(-\int \Delta R_s(i_s + \Delta i_s)dt\right) \otimes (i_s + \Delta i_s) \tag{29}$$

The pervious equation gives the change in electromagnetic torque as a function of changes in stator current and stator resistance. It also shows that the torque, current, and stator resistance errors are all related. In this section, the difference between the actual current vector and the estimated current vector will be used to compensate the change in the stator resistance. The estimated current vector can be derived from the estimated torque and active flux based on the motor current model. The d-axis current component can be estimated from the active flux magnitude as follows:

$$\hat{i}_{dm} = \frac{\lambda_a - \lambda_f}{L_d - L_q} \tag{30}$$

Combining equations (30) and (9), the q-axis current is estimated from:

$$\hat{i}_{qm} = \frac{\hat{T}_e}{1.5P(\lambda_f + (L_d - L_q)\hat{i}_{dm})} \tag{31}$$

Using equations (30) and (31) the magnitude of the stator current (neglect the iron loss current components) is estimated as:

$$\hat{i}_s = (\hat{i}_{dm}{}^2 + \hat{i}_{qm}{}^2)^{0.5} \tag{32}$$

The error between the estimated and actual current vectors can be expressed as follows:

$$e(k) = \hat{i}_s(k) - i_s(k) \tag{33}$$

The change in current error will become:

$$\Delta e(k) = e(k) - e(k-1) \tag{34}$$

The current error and the change in current error are used as inputs to a fuzzy logic estimator in order to predict the change in the stator resistance ΔR_s. Each of the input and output variables to the fuzzy logic block are divided into seven fuzzy segments, namely, NL, NM, NS, ZE, PS, PM, and PL. The range of control (or universe of discourse) for stator current error is chosen between 0.1A and - 0.1A, and its change is chosen between 0.05 and -0.05 amp. Also, the change in stator resistance is chosen between 0.05 and -0.05 ohm. Triangular functions are used for membership distribution. Figure 8 shows the membership distribution for the current error, change in current error and change in stator resistance. Fuzzy rules are selected to give the variation in the stator resistance. Each control rule can be described using the input variables $e(k)$, $\Delta e(k)$ and the output variable ΔR_s.

The i^{th} rule r_i can be expressed as:

r_i: if e is A_i, Δe is B_i, then ΔR_s is N_i (35)

where A_i, B_i, N_i are the fuzzy subsets. The total number of rules is 49 rule which are given in table 1. The interface method used in this paper is Mamdani's procedure. The firing strength α_i for ith rule is expressed as:

$$\alpha_i = \min(\mu(e), \mu(\Delta e)) \tag{36}$$

where $\mu(e)$ and $\mu(\Delta e)$ are the membership grade of the current error and the change in the current error, respectively. The membership function of the resultant

aggregation is obtained by the maximum method. The maximum method takes the maximum of their degree of support (DoS) values.

In the defuzzification stage, a crisp value for the output variable (change in resistance ΔR_s) is obtained using the mean of maximum (MoM) operator [25]. The change in the stator resistance (ΔR_s) is added to the previously estimated resistance. The block diagram of the stator resistance estimator is shown in figure 9.

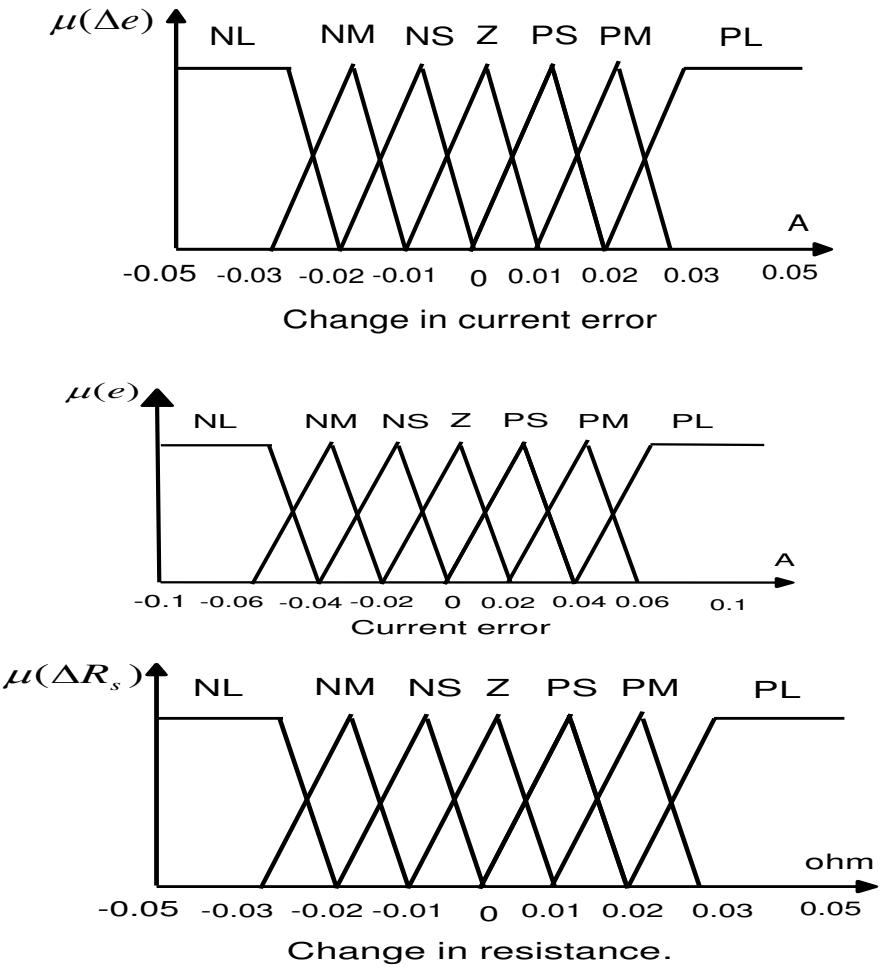

Figure 8: Input and output membership functions of the fuzzy logic estimator.

The block diagram of the speed proposed sensorless torque/flux sliding mode controller of the IPMSM is shown in figure 10. In this figure, the stator flux vector and the motor torque are estimated from the measured voltage and current signals. The rotor speed and position angle are estimated based on the active flux. The SMC is designed to generate the stator reference voltage based on the torque and flux errors as in Ref. [27]. Space vector modulation is used to generate the inverter firing signals based on the reference value of the stator voltage in addition to the constant switching frequency. Two level three phase inverter is used to feed the IPMSM. The iron loss

and saturation effect are taken in the motor modeling. No additional measurements or axis transformation are required.

Table 1: Fuzzy rules for the fuzzy resistance estimator

$e(k)$ / $\Delta e(k)$	NL	NM	NS	Z	PS	PM	PL
NL	NL	NL	NL	NL	NM	NS	Z
NM	NL	NL	NL	NM	NS	Z	PS
NS	NL	NL	NM	NS	Z	PS	PM
Z	NL	NM	NS	Z	PS	PM	PL
PS	NM	NS	Z	PS	PM	PL	PL
PM	NS	Z	PS	PM	PL	PL	PL
PL	Z	PS	PM	PL	PL	PL	PL

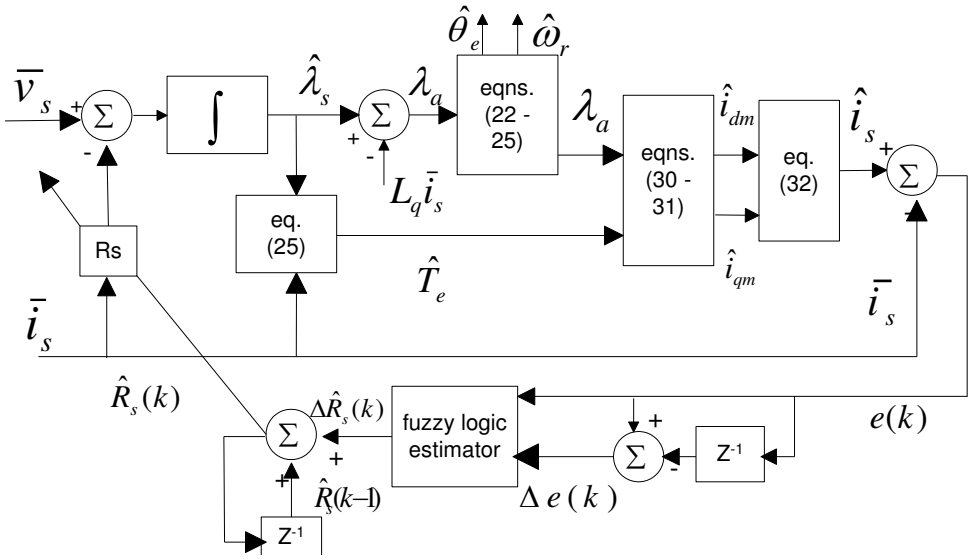

Figure 9: Block diagram of the stator resistance fuzzy logic estimator.

5. RESULTS AND DISCUSSIONS

Simulation results are carried out to evaluate the performance of the proposed scheme. The self and cross coupling inductances variation are taken into the motor model, while the self inductance variation only is considered in the observer design. The simulations are carried out to evaluate the performance of the proposed scheme at standstill, low and high speed operation with load disturbance and stator resistance variation in the presence of core loss and saturation. The simulation results are compared with those measured in the literature [11] to evaluate the validity of the proposed scheme. In [11],

a high frequency signal injection technique and a sliding mode observer are companied together to estimate the rotor speed, position and stator resistance of the IPMSM. However, the scheme in [11] is more complex compared to the proposed scheme. The IPMSM parameters used in the proposed and pervious schemes are the same and given in appendix I.

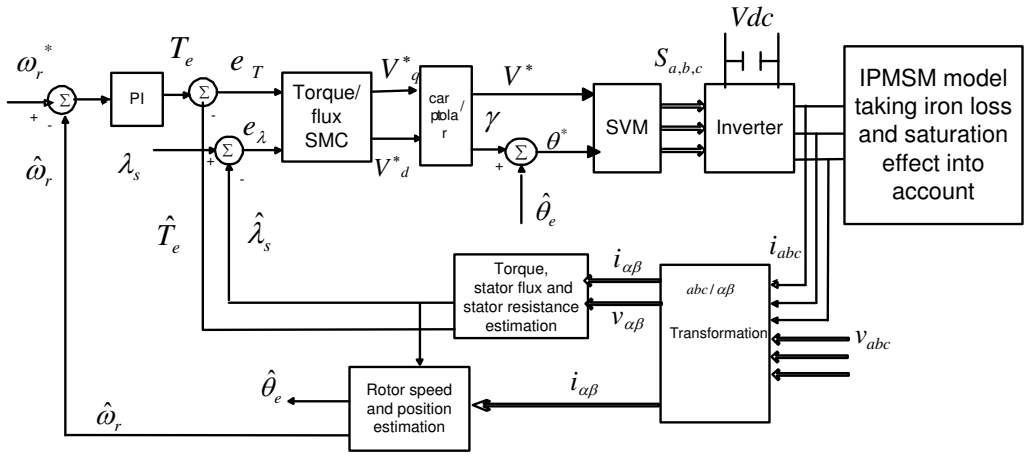

Figure 10: Block diagram of the proposed sensorless torque/ flux SMC.

5.1 Drive operation at high speed and load disturbance

The motor was initially running at 1000 rpm under no load condition, and full load torque was applied at t = 2.5 s. Figure 11a shows the dynamic speed response of the proposed scheme taking saturation and iron loss into account. It is shown that a dip occurred in the motor speed when the load torque increased. The figure shows that the dip in the rotor speed is very small during the transient interval and quickly decays to zero. In addition, the figure shows the quadrature axis self inductance variation at high load torque. Figure 11b shows the actual speed, estimated speed and position error of the scheme proposed in the literature [11]. By comparing the figures, it is noticed that the simulation and experimental results agree to some extent under the same operating conditions. In addition, taking the saturation effect and iron loss into account improves the theoretical results.

5.2 Drive operation at very low reversible speed

In this case, the reference speed is reversed from − 5 to 5 rpm with full load torque applied. Figure 12a shows the simulation results of the proposed scheme under these conditions. As shown in the figure, the estimated speed follows the actual speed very well during the reversal operation. The position estimation error is very small, which confirms the effectiveness of the proposed algorithm. Figure 12b shows the experimental results in the literature [11]. As shown in the figure, some oscillations appear in the actual and estimated speed waveforms. These oscillations may be as a result of the chattering phenomena of sliding mode observer.

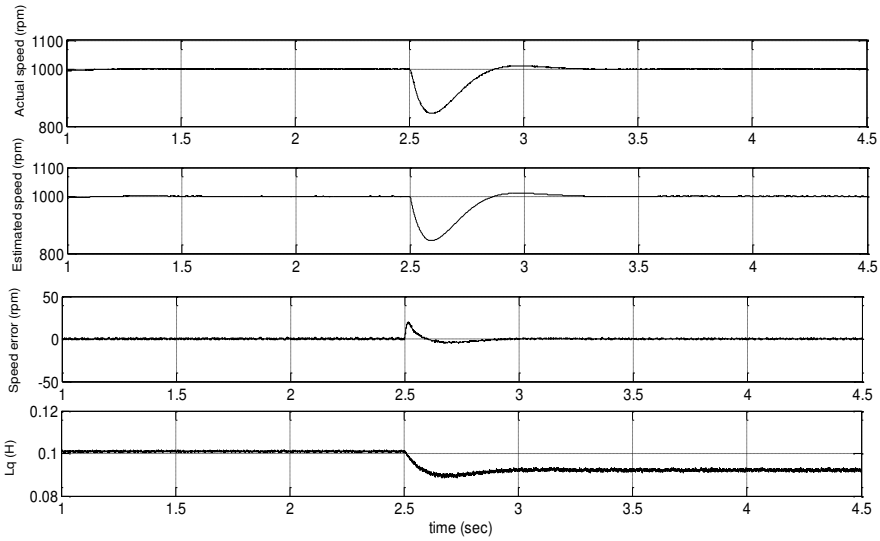

(a)

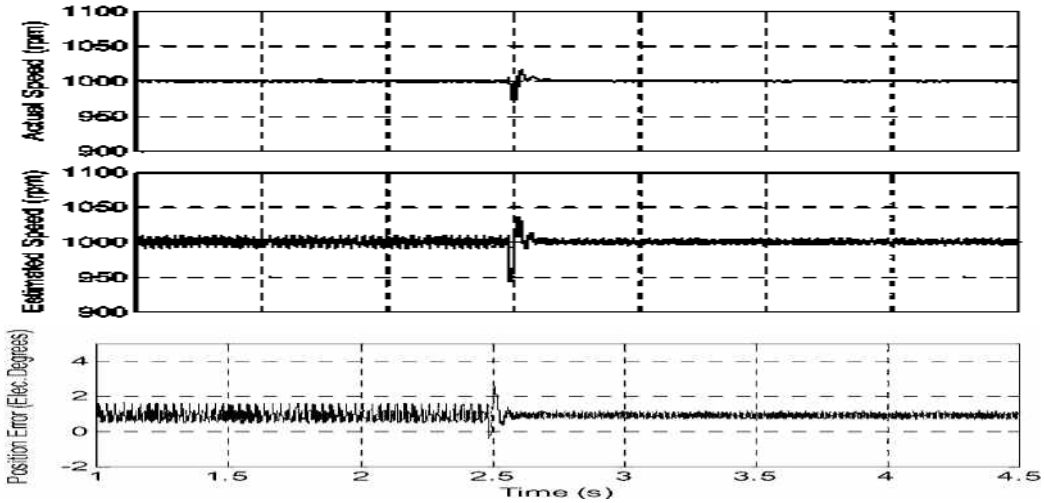

(b)

Figure 11: Actual speed, estimated speed, speed error and position error at high speed. (a) The active flux with taking saturation effect and iron loss into account (simulation) (b) The high frequency injection and sliding mode observer (experimental).

5.3 Drive performance at standstill

Figure 13a and b shows the measured speed, estimated speed and position error waveforms of the proposed scheme and the pervious one [11] respectively, at zero speed operation with full load torque steps. The load was initially applied to the motor at t = 0.5 sec. and was subsequently removed at t = 2.75 sec. Figure 13a shows that the perturbation in the rotor speed is small, even during load dynamics. It is observed that the estimated speed tracks the actual speed very well and the position estimation error is very small during transients and steady state. Small dips occurred in the actual and estimated speeds of the proposed scheme during load disturbance. Hence, the proposed

scheme is capable of persistent zero-speed operation with full load torque. In figure 13b, the actual and estimated speed waveforms of the experimental results have some oscillations as a result of the chattering of the sliding mode observer.

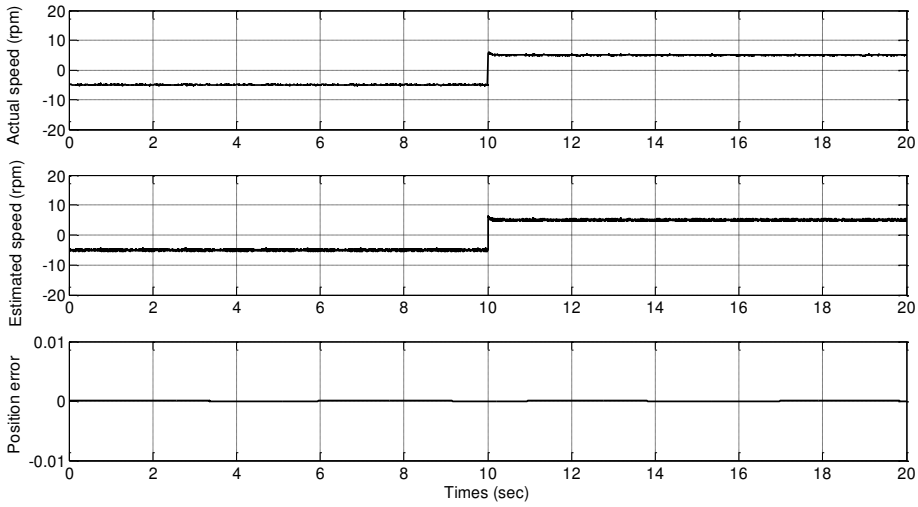

(a)

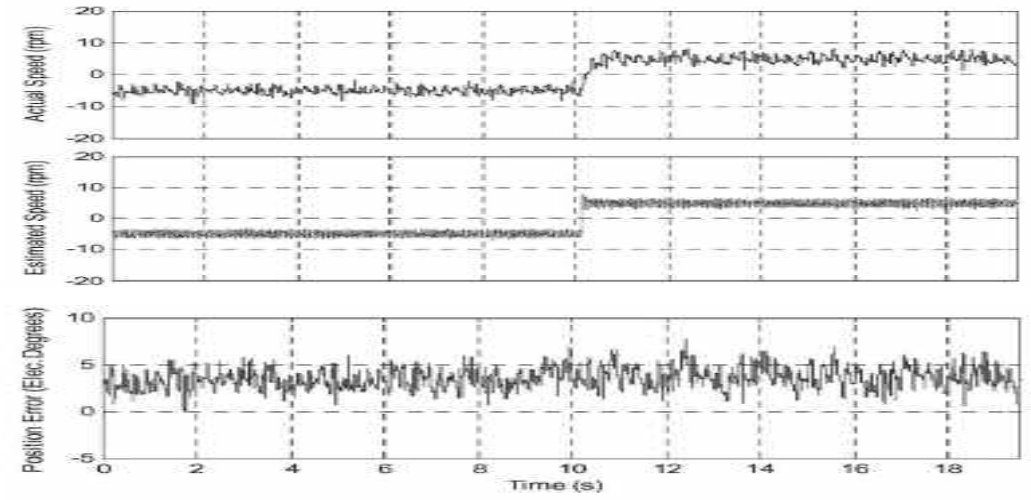

(b)

Figure 12: Actual speed, estimated speed and position error at standstill operation.
(a) The active flux -SMC taking saturation effect and iron loss into account (simulation).
(b) The high frequency injection and sliding observer (measured).

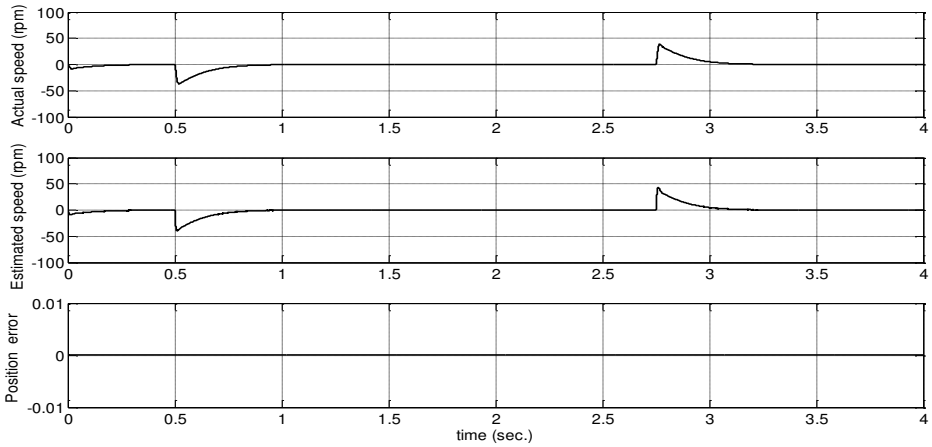

(a)

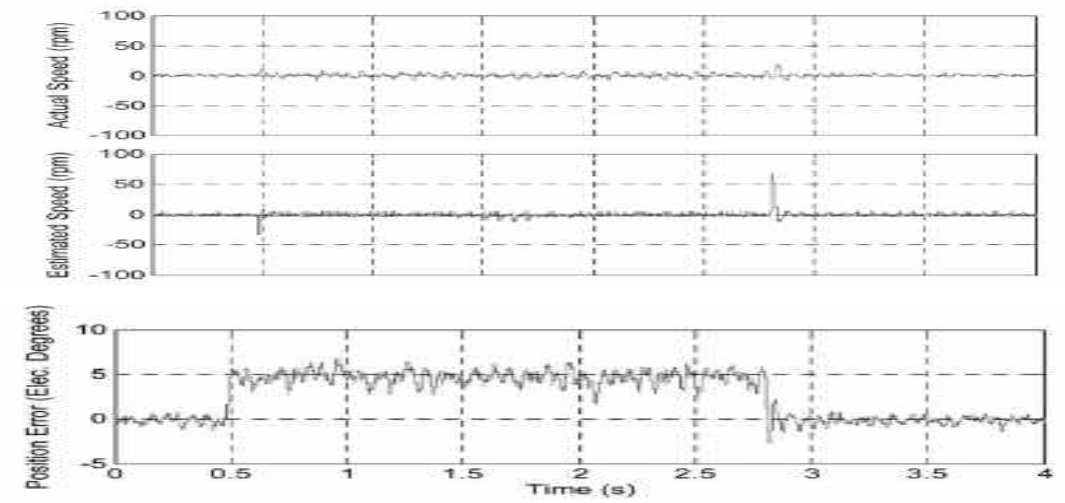

(b)

Figure 13: Actual speed, estimated speed and position error at standstill operation
(a) The active flux (simulation)
(b) the high frequency injection (experimentally)

5.4 Drive performance at stator resistance variation

Figure 14a shows the response of the proposed drive due to a step change in stator resistance without stator resistance estimation. The motor was running under half full load condition at 500 rpm when the stator resistance was increased steeply by 40% at t = 1.15 sec. The actual speed, estimated speed and speed estimation error waveforms of the proposed scheme are shown in the figure, respectively. The figure shows oscillations in the actual and estimated speed waveforms. If a stator resistance estimation algorithm is used, the speed oscillation will disappear as shown in figure 14b. The figure shows that the actual and estimated resistances are aligned. Figure 15c shows the scheme performance when the saturation and iron loss are taken into account. A small oscillation appears in the estimated speed and the estimated resistance

at the instant of stator resistance variation. However, these oscillations are damped quickly. Figure 15d shows the estimated stator resistance and speed estimation errors of the scheme in literature [11]. The resistance adaptation law is able to precisely identify the stator resistance in less than 1 sec. By comparing figures 14c and 14d, it is shown that the proposed fuzzy estimator response is faster than that in the literature.

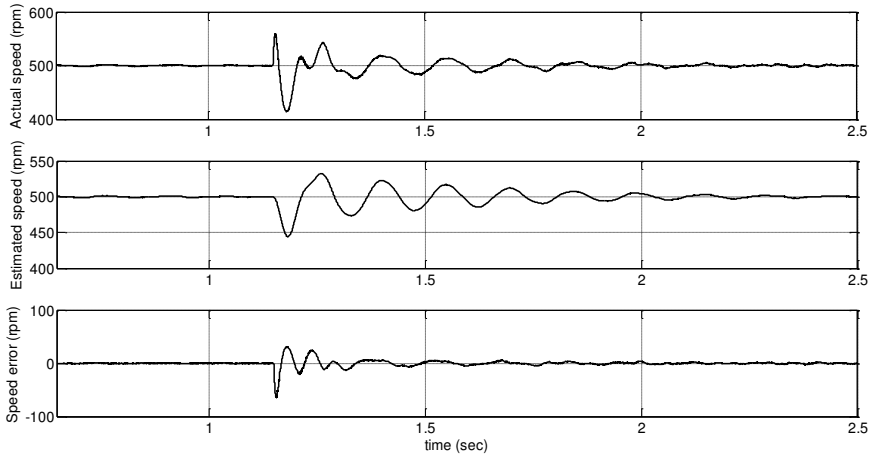

(a)

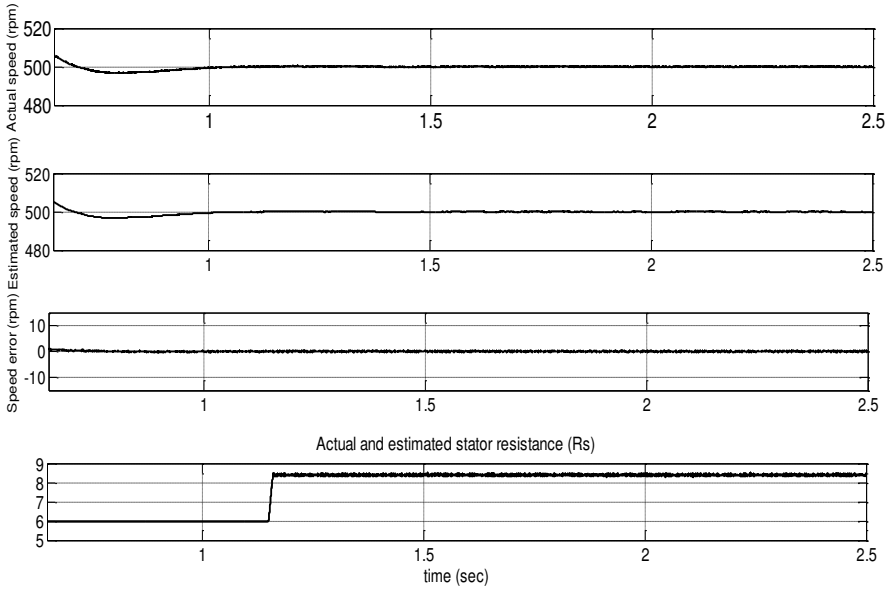

(b)

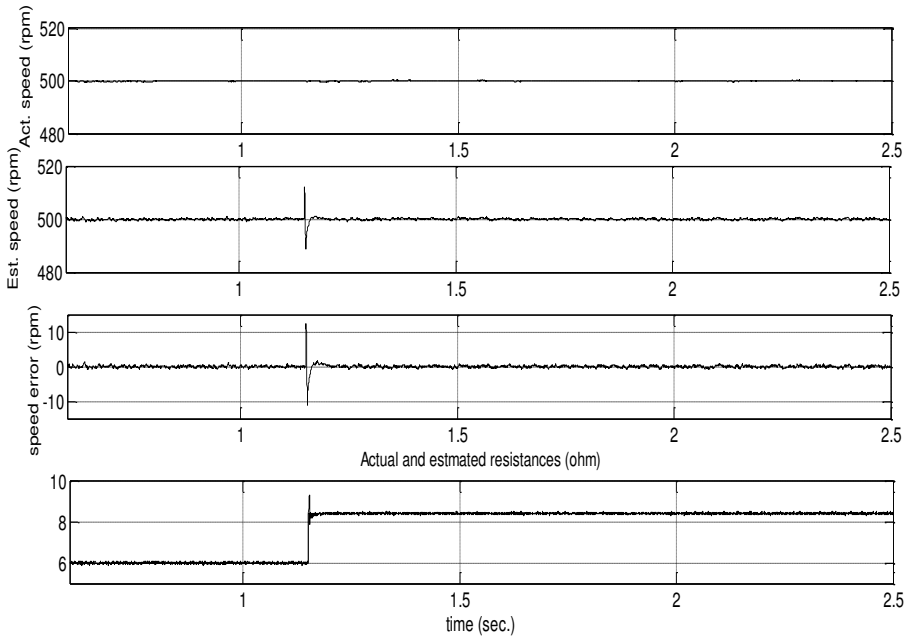

(c)

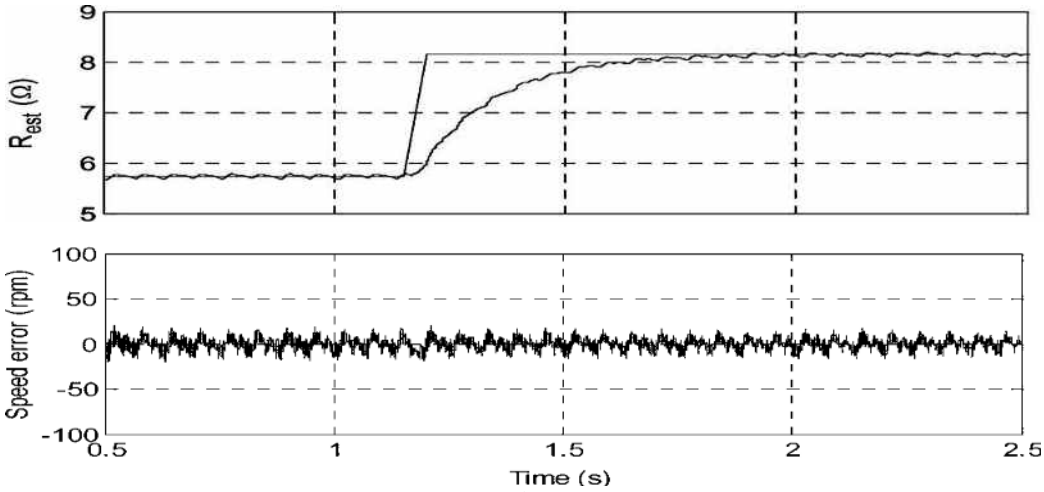

(d)

Figure 14: Stator resistance variation effect on the scheme performance:
(a) Without stator resistance estimation and saturation effect and iron loss into account.
(b) With stator resistance estimation and without saturation effect and iron loss into account.
(c) With stator resistance estimation and taking saturation and core loss into account.
(d) The high frequency injection and sliding mode observer (experimental).

6. CONCLUSION

In this paper, the speed sensorless control of the IPMSM based on direct torque control is studied. The rotor speed and position was estimated online based on active flux concept. The effect of the saturation and iron loss were taken into account to improve the theoretical results. To improve the classical DTC performance, a sliding mode controller combined with SVM was used to replace the classical hysteresis controllers and lookup table of DTC. In addition, a fuzzy logic estimator was proposed to estimate the stator resistance variation online. To evaluate the performance of the proposed scheme, simulation works were carried out and compared with published results. From the present analysis and simulation results, one can draw the following main conclusions:

1- The speed estimation algorithm based on active flux concept gives accurate estimation of the rotor speed and position at standstill, low and high speed operation. The estimated and actual motor speeds can trace well the reference value. The speed and position errors of the proposed scheme are low compared to the published results.
2- Speed reversal operation of the proposed scheme is studied. The motor speed and the estimated speed are aligned. The speed and position error are small. Also, the simulation results agree with the experimental results.
3- For speed estimation based on active flux concept, the stator inductance variation due to saturation phenomena can cause unacceptable performance. On the other hand, taking inductance variation into account improves the calculated results.
4- The fuzzy logic estimator can detect well the thermal variation of the stator resistance. The estimation error is very low during a ramp or step variation of the stator resistance. Compared to the published results, the proposed fuzzy estimator is faster and more accurate than the sliding mode observer.

APPENDIX I

Parameters and data of the IPMSM

Rated power (W)	1000	Rated phase voltage (V)	132
R_s (Ω)	5	Magnet flux linkage λ_f (Wb)	0.533
L_q (H)	0.1	Rated torque Te (N.m)	6
L_d (H)	0.05	DC voltage (V)	300
No. of pole pairs	2	Base speed (rpm)	1500

REFERENCES

[1] Jochim Holtz, " Sensorless control of induction machines with or without signal injection" IEEE Trans. on Indust. Electron. , Vol. 53, No. 1, February 2006, pp.7-30.
[2] Shigeo Morimotor, Keisuke Kawamoto, Masayuki Sanada, and Yoji Takeda, " Sensorless control strategy for salient pole PMSM based on extended EMF in

rotating frame" *IEEE* Trans. on Indust. Appl., Vol. 38, No. 4, July/Augst 2002, pp. 1054-1061.

[3] Zhiqian Chen, Muyuwo Tomita, Shinji Doki, and Shigeru Okuma, " An extended electromotive force model for sensorless control of interior permanent magnet synchronous motors" IEEE Trans. on Indust. Electron., Vol. 50, No. 2, April 2003, pp. 288-295.

[4] Shinji Ichikawa, Muyuwo Tomita, Shinji Doki, and Shigeru Okuma, " Sensorless control of permanent magnet synchronous motors using online parameters identification based on system identification theory" IEEE Trans. on Indust. Electron., Vol. 53, No. 2, April. 2006, pp. 363-372.

[5] Shigeo Morimotor, Masayuki Sanada and Yoji Takeda, " Mechincal sensorless drives of IPMSM with online parameter identification" IEEE Trans. on Indust. Appl., Vol. 42, No. 5, October 006, pp. 1241-1248.

[6] Satoshi Ogasawara and Hirofumi Akagi, "Implementation and position control performance of a position sensorless IPM motor drive system based on magnetic saliency" IEEE Trans. on Indust. Appl., Vol. 34, No. 4, July/Augst. 1998, pp. 806-812.

[7] Antti Piippo, Mark I Iinkkanen, and Jorma Luomi, " Adaptation of motor parameters in sensorless PMSM drives" IEEE Trans. on Indust. Appl., Vol. 45, No. 1, January/February . 2009, pp. 203-212.

[8] Chan-Hee Choi and Jul-Ki Seok, "Pulsating signal injection based axis switching sensorless control of surface mounted permanent magnet motors for minimal zero current clamping effects" IEEE Trans. on Indust. Appl., Vol. 44, No. 6, Nov/Dec. 2008, pp. 1741-1748.

[9] Cristian Lascu, Ion Boldea and Frede Blaabjerg, " Direct torque control of sensorless induction motor drives: a sliding-mode approach" IEEE Trans. on Indust. Appl., Vol. 40, No. 2, March/April 2004, pp. 532-590.

[10] Gheorghe-Daniel Andreescu, Cristian Ilie Pitic, Frede Blaabjerg and Ion Boldea, "Combined flux observer with signal injection enhancement for wide speed range sensorless direct torque control of IPMSM drives" IEEE Trans. on Energy Conversion, Vol. 23 No.2, June 2008, pp. 393- 402.

[11] Gilbert Foo, and M. F. Rahman, “Sensorless Sliding-Mode MTPA Control of an IPM Synchronous Motor Drive Using a Sliding-Mode Observer and HF Signal Injection” IEEE Trans. on Indust. Electron, Vol. 57, No. 4, April 2010, pp. 1270-1278.

[12] Zhiqian Chen, Muyuwo Tomita, Shinji Doki, and Shigeru Okuma, "New adaptive sliding mode observers for position- and velocity-sensorless controls of brushless motors" IEEE Trans. on Indust. Electron., Vol. 47, No. 3, July 2000, pp. 582-591.

[13] Mohamed Boussak, "Implementation and experimental investigation of sensorless speed control with initial rotor position estimation for interior permanent magnet synchronous motor drive" IEEE Trans. on Indust. Electron., Vol. 20, No. 6, November 2005, pp. 1413-1422.

[14] YongLiu, Zi Qiang Zhu and David Howe, "Instantaneous torque estimation in sensorless direct-torque-controlled brushless DC motors" IEEE Trans. on Indust. Appl., Vol. 42, No. 5, September/October 2006, pp. 1275-1283.

[15] Zhuang Xu. and M.A. Rahman, " An adaptive sliding stator flux observer for a direct-torque-controlled IPM synchronous motor drive" IEEE Trans. on Indust. Electron., Vol.54, No.5, October 2007, pp. 2398-2406.

[16] Masaru Hasegawa and Keiju Matsui, " IPMSM position sensorless drives using robust adaptive observer on stationary reference frame" IEEJ Trans. on Electrical and Electronic Eng. 2008, Vol. 3, pp. 120-127.

[17] Masaru Hasegawa, Satoshi Yoshioka and Keiju Matsui, " Position sensorless control of interior permanent magnet synchronous motors using unknown input observer for high speed drives" IEEE Trans. on Indust. Appl., Vol. 45, No. 3, May/June 2009, pp. 938-946.

[18] Kyo-Beum Lee and Frede Blaabjerg, " Sensorless DTC-SVM for induction motor driven by a matrix converter using a parameter estimation strategy" IEEE Trans. on Indust. Electron., Vol. 55, No.2, February 2008, pp. 512-521.

[19] Muhammed Fazlur Rahman, L. Zhong, Md.Enamul Haque and M.A. Rahman, " A direct torque-controlled interior permanent magnet synchronous motor drive without a speed sensor" IEEE Trans. on Energy Convers., Vol.18, No.1, March 2003, pp. 17-22.

[20] Miran Rodic and Karel Jezernik, "Speed-Sensorless sliding mode torque control of an induction motor" IEEE Trans. on Indust. Electron., Vol. 49, No. 1, February 2002, pp. 87-95.

[21] Ion Boldea, Mihaela Codruta Paicu, Gheorghe-Daniel Andreescu, and Frede Blaabjerg, ""Active flux" DTFC-SVM sensorless control of IPMSM" IEEE Trans. on Energy Convers., Vol. 24. No.2, June 2009, pp. 314-322.

[22] Bojan Stumberger, Gorazd Stumberger, Drago Dolinar, Anton Hamler, and Mladen Trlep, “Evaluation of Saturation and Cross-Magnetization Effects in Interior Permanent-Magnet Synchronous Motor” IEEE Trans. on Industry Applic., Vol. 39, No. 5, Sept./Oct. 2003, pp. 1264-1270.

[23] Naomitsu Urasaki, Tomonobu Senjyu, and Katsumi Uezato, “ Relationship of Parallel Model and Series Model for Permanent Magnet Synchronous Motors Taking Iron Loss Into Account” IEEE Trans. on. Energy Conversion, Vol. 19, No. 2, June 2004, pp. 265-270.

[24] Y.–K. Chin, and J. Soulard, "Modeling of iron losses in permanent magnet synchronous motors with fields weakening capability for electric vehicles" International Journal of Automation Technology, Vol.4. No. 2, 2003, pp. 87-94.

[25] Sayeed Mir, Malik E. Elbuluk, and Donald S. Zinger, " PI and fuzzy estimators for tuning the stator resistance in direct torque control of induction machines" IEEE Trans. on Power Electron., Vol. 13. No.2, March 1998, pp. 279-287.

[26] Baburaj Karanayil, and Muhammed F. Rahman "Stator and rotor resistance observers for induction motor drive using fuzzy logic and artificial neural networks" IEEE Trans. on Energy Convers., Vol. 20, No. 4, December 2005, pp. 771-780.

[27] A. A. Hassan, A. M. El-Sawy, Y. S. Mohamed, and E. G. Shehata “ Design of A Recurrent Neural Controller for PMSM Drive Based on Sliding Mode Torque Control” International Review of Automatic Control Journal (IREACO), Italy, January 2011.

التحكم في عزم المحرك التزامني ذو الأقطاب المغناطيسية الدائمة بدون حساس سرعة مع الأخذ في الإعتبار تأثير المفاقيد الحديدية و التشبع المغناطيسي

هذا البحث يبحث تحكم مباشرفى عزم المحرك التزامنى ذو الأقطاب المغناطيسية الدائمة (Direct torque control) بدون حساس السرعة أعتمادا على نظام المتحكم الأنزلاقى. تحسب سرعة و زاوية العضو الدوار للمحرك بناء على مفهوم الفيض الفعال. يحتاج حساب الفيض الفعال الى قيمة الحث الذاتى فى الأحداثى العمودى للعضو الثابت للمحرك. لذلك تم تعديل نموذج المحرك لأخذ تأثير ظاهرة التشبع على الحث الذاتى فى الأحداثيين المباشر والعمودى للمحرك. حيث تم تخزين قيم تغير الحث الذاتى فى الأحداثيين المباشر و العمودى مع التيار فى جدول داخل النموذج. كما انه تم أخذ مقاومة القلب الحديدى للمحرك فى الأعتبار لتحسين النتائج النظرية. للتغلب على التموجات العالية التى تعيب نظام التحكم المباشر فى العزم يتم أستخدام متحكم أنزلاقى للتحكم فى العزم و الفيض المغناطيسى للمحرك. و قد تم أستخدام دالتى تكامل لتصميم المتحكم الأنزلاقى. حيث يقوم المتحكم بحساب الجهد من الفرق بين العزم المطلوب و الفعلى و الفرق بين كثافة الفيض المغناطيسى و الفعلى اعتمادا على دالتى التكامل. و لضمان ثبات النظام أثناء زاوية الوصول تم أستخدام فكرة المتحكم الأنزلاقى الكلى. كما تم أضافة نظام ضبط المتجه الفراغى (Space vector modulation) للحصول على أقل تموجات فى العزم و الفيض المغناطيسى للمحرك و زيادة نقاوة الجهد. النظام المقترح يتميز بالبساطة و عدم الحاجة الى نظام حقن خارجى. وللحكم على اداء التحكم المقترح تم عمل محاكاة بالكمبيوتر عند ظروف تشغيل مختلفة. حيث أوضحت النتائج الأداء المتميز للنظام المقترح عند البدء و السرعات البطيئة و العالية مع تغير معاملات المحرك او الحمل على المحرك. كما تم مقارنة النتائج النظرية مع نتائج عملية منشورة سابقا لتوضيح كفاءة أداء النظام المقترح.